Supporting Information

Andersen et al. 10.1073/pnas.1709581114

Methods

Bishop Tuff Samples. Samples of fall units are composites, F6 and F7 of several 4- to 6-cm primary pumice blocks and unit F3 of primary pumice blocks and lapilli sieved to >4 mm with lithic fragments removed by handpicking. All are crystal-poor normal-type rhyolite pumice, following the classification scheme of Hildreth and Wilson (16). Each ignimbrite sample comprises a single 20-cm pumice block. The Ig1Eb sample is of the crystal-rich normal variety, whereas the Ig2Nb sample is an adobe-type pumice. All samples were washed in deionized water before processing, and care was taken to remove adhering ignimbrite matrix from the Ig1Eb and Ig2Nb samples.

^{40}Ar/^{39}Ar Age Determinations. Sanidine phenocrysts were separated from the Bishop Tuff ignimbrite and fall samples by gentle crushing and handpicking followed by soaking in cold, dilute HF in an ultrasonic bath and repeated washes in deionized water. Final selection of grains was performed under a binocular microscope to isolate inclusion-free crystals. Large (>1 mm) sanidine crystals were targeted in all samples but were scarce in fall unit F2; consequently, sanidines in this unit were isolated from the 0.5- to 1-mm sieve fraction using standard density and magnetic techniques.

Sanidine separates were irradiated in Al disks in the Cd-lined in-core irradiation tube (CLICIT) of the Oregon State University TRIGA (Training, Research, Isotopes, General Atomics) reactor. The neutron fluence monitor was Alder Creek Rhyolite sanidine (age = 1.1864 ± 0.003/0.012 Ma) (11, 23). Reactor-induced isotopic production ratios for this irradiation were $(^{36}Ar/^{37}Ar)_{Ca} = 2.65 \pm 0.02 \times 10^{-4}$, $(^{38}Ar/^{37}Ar)_{Ca} = 1.96 \pm 0.08 \times 10^{-5}$, $(^{39}Ar/^{37}Ar)_{Ca} = 6.95 \pm 0.09 \times 10^{-4}$ (54); $(^{38}Ar/^{39}Ar)_{K} = 1.210 \pm 0.002 \times 10^{-2}$, $(^{40}Ar/^{39}Ar)_{K} = 5.4 \pm 1.4 \times 10^{-4}$ (55). The atmospheric ^{40}Ar/^{36}Ar = 298.56 ± 0.31 ratio is from Lee et al. (29) and decay constants are those of Min et al. (48).

Individual sanidine phenocrysts were incrementally heated with a Photon Machines 60W CO_2 laser. Gas released from each heating step was cleaned with two SAES GP50 getters, at 450 °C and room temperature, for 60 s, followed by exposure to an ARS cryotrap at −125 °C for 60 s. Blank and standard gas analyses follow the same gas cleanup routine. The analytical sequence comprises repeated sets of blank–standard–sample; thus all sample analyses are bracketed by pairs of standards and blanks. Isotopic measurements were performed using a Nu Instruments Noblesse 5 collector mass spectrometer fitted with ion counting (IC) multipliers using a routine involving one peak hop following the methods of Jicha et al. (11) with two minor modifications: (*i*) A separate set of quad lens settings were used following the peak hop so that $^{37}Ar_{IC2}/^{39}Ar_{IC1}$ and $^{36}Ar_{IC2}/^{38}Ar_{IC1}$ are measured in the same position in collectors IC2 and IC1; (*ii*) the ^{40}Ar/^{39}Ar ratio was determined by measuring ^{40}Ar in collector IC0 and ^{39}Ar in collector IC1 and the measured $^{40}Ar_{IC0}/^{39}Ar_{IC1}$ ratio based on the $^{40}Ar_{IC0}/^{39}Ar_{IC1}$ of the bracketing standard gas analyses. Analysis of the standard gas aliquots allows the calculation of correction factors, which incorporate mass discrimination of the source and detector, and detector efficiency. By analyzing the standard gas approximately every 45 min throughout the analytical session, any drift in the source or detectors is well characterized. Complete ^{40}Ar/^{39}Ar analytical data including age spectrum and isochron plots are provided in Datasets S1–S3.

Plateau and isochron calculations were performed using Isoplot (56). A plateau is defined as at least three consecutive, mutually concordant steps that comprise at least 50% of the ^{39}Ar released. Additionally, the weighted mean must fit the plateau steps with at least a 5% probability of fit, an error-weighted line defined by the plateau steps does not have a slope significantly different from zero with 5% confidence, the outermost of six or more steps are not significantly different from the weighted mean (at 1.8σ), and the outermost two steps for a plateau of nine or more steps do not have a nonzero slope (at 1.8σ).

Excess Ar Sensitivity. The curves in Fig. 4*A* illustrate the predicted offset of the isochron intercept from the atmospheric ^{40}Ar/^{39}Ar ratio due to the presence of excess Ar required to produce an age offset of Δt. These curves are constructed by first calculating the concentration (moles per gram) of radiogenic Ar (^{40}Ar*) and excess Ar for a given offset from the eruption age ($^{40}Ar_{xs}^{\Delta t}$) based on the radioactive decay of ^{40}K,

$$^{40}\mathrm{Ar}^{*} = {}^{40}K\left(\frac{\lambda_{ec}}{\lambda_{tot}}\right)\left(e^{\lambda_{tot}t}-1\right) \quad \text{[S1]}$$

$$^{40}\mathrm{Ar}_{xs}^{\Delta t} = {}^{40}K\left(\frac{\lambda_{ec}}{\lambda_{tot}}\right)\left(e^{\lambda_{tot}\Delta t}-1\right), \quad \text{[S2]}$$

where ^{40}K is the concentration in sanidine (moles per gram) and assumes an average BT sanidine K_2O content of 10.9 wt. % (37), λ_{ec} is the decay constant for ^{40}K decay to ^{40}Ar by electron caption, λ_{tot} is the total decay constant for ^{40}K, t is the eruption age taken here to be 764.8 ka, and Δt is the offset from the eruption age. Then, the atmospheric ^{40}Ar and ^{36}Ar concentrations (moles per gram) are calculated from a specified $^{40}Ar_{atm}/^{40}Ar^{*}$ ratio (f_{atm}) and the atmospheric ^{40}Ar/^{36}Ar ratio of Lee et al. (29), 298.56.

$$^{40}\mathrm{Ar}_{atm} = f_{atm}^{40}\mathrm{Ar}^{*} \quad \text{[S3]}$$

$$^{36}\mathrm{Ar} = \frac{^{40}\mathrm{Ar}_{atm}}{298.56}. \quad \text{[S4]}$$

The deviation of the isochron intercept from the atmospheric ^{40}Ar/^{36}Ar ratio is then calculated as

$$\Delta\text{intercept} = \frac{^{40}\mathrm{Ar}_{atm} + {}^{40}\mathrm{Ar}_{xs}^{\Delta t}}{^{36}\mathrm{Ar}} - 298.56. \quad \text{[S5]}$$

Ar Diffusion Modeling. The evolution of the Ar concentration of a sanidine crystal is modeled as 3D isotropic volume diffusion with simultaneous radioactive decay. The distribution of ^{40}Ar in space and time is calculated by

$$\frac{\partial C}{\partial t} = D\nabla^2 C + {}^{40}K\left(\frac{\lambda_{ec}}{\lambda_{tot}}\right)\left[e^{(\lambda_{tot}t)}-1\right], \quad \text{[S6]}$$

where C is the concentration of ^{40}Ar, t is time, D is the temperature-dependent diffusion constant of Ar in sanidine, λ_{ec} is the decay constant for ^{40}K decay to ^{40}Ar by electron caption, and λ_{tot} is the total decay constant for ^{40}K. The decay constants of Min et al. (48) are used to calculate radiogenic Ar ingrowth. The diffusion constant is calculated by

$$D = e^{\left[\log(D_0)-\frac{Ea}{RT}\right]}, \quad \text{[S7]}$$

where D_0 is the frequency factor, E_a is the activation energy, R is the ideal gas constant, and T is the temperature in Kelvins. The activation energy and effective domain size governing Ar diffusion in K feldspar is controversial (53, 58). The models shown in Fig. 4*C* are calculated using $E_a = 198.2$ kJ/mol and $D_0 = 3.74 \times 10^{-6}$ m^2/s for $T < 725$ and $E_a = 268$ kJ/mol and $D_0 = 0.0055$ m^2/s for $T \geq 725$ (53) and assume a diffusion domain similar to the crystal size (53, 58). Models were also calculated using a lower E_a and smaller diffusion domain (r): $E_a = 192.5$ kJ/mol, $D_0/r^2 = 5$ s^{-1}, and $r = 6$ μm (57). These parameters yield shorter diffusion timescales (Fig. S2) but do not substantially alter our interpretations.

Eq. **S6** is solved using a finite difference algorithm. The diffusion calculation is carried out over one octant of a 2-mm cube and assumes reflection symmetry across the x–y, x–z, and y–z planes. The initial Ar concentration is calculated by 10 ky to 80 ky of radioactive decay using the average BT sanidine K_2O composition of 10.9 wt. % (37). This initial Ar content is evenly distributed within the crystal and does not include an excess or atmospheric Ar component. The boundary at the interior of the crystal assumes symmetric diffusion, and the surrounding magma chamber is assumed to be Ar-free. A 1D transect of the numerical model result is validated against the analytical expression for diffusive loss from an infinite sheet (Fig. S4),

$$C(x,t) = C_0\left[\mathrm{erf}\left(\frac{x}{\sqrt{Dt}}\right)\right], \qquad \textbf{[S8]}$$

where C_0 is the initial ^{40}Ar* concentration of the crystal and x is the distance from the rim.

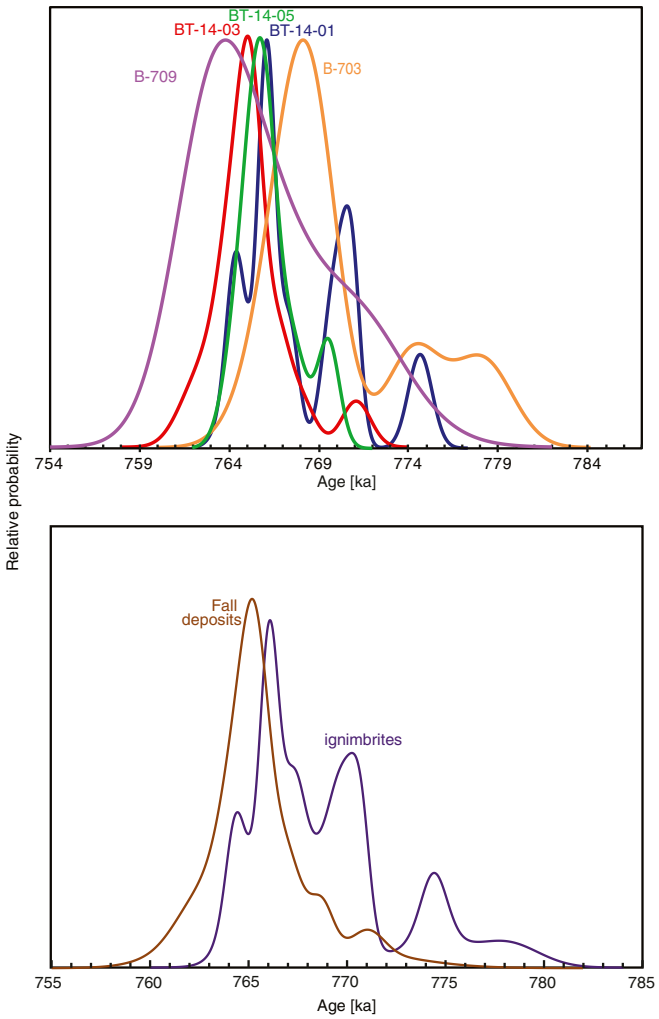

Fig. S1. Probability density curves comparing the age populations of each BT sample and of the three fall deposit samples to the two ignimbrite samples. The ignimbrite samples have a higher proportion of sanidine that produces preeruption dates.

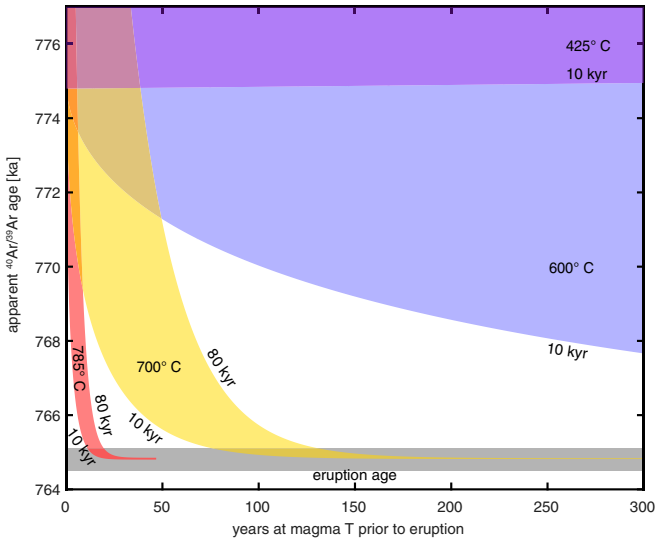

Fig. S2. Diffusion models calculated using the mean parameters of Lovera et al. (57). These calculations predict a lower temperature of $^{40}Ar^*$ accumulation and shorter timescales of preeruption storage compared with those in Fig. 4*C*, but do not substantively alter our conclusions.

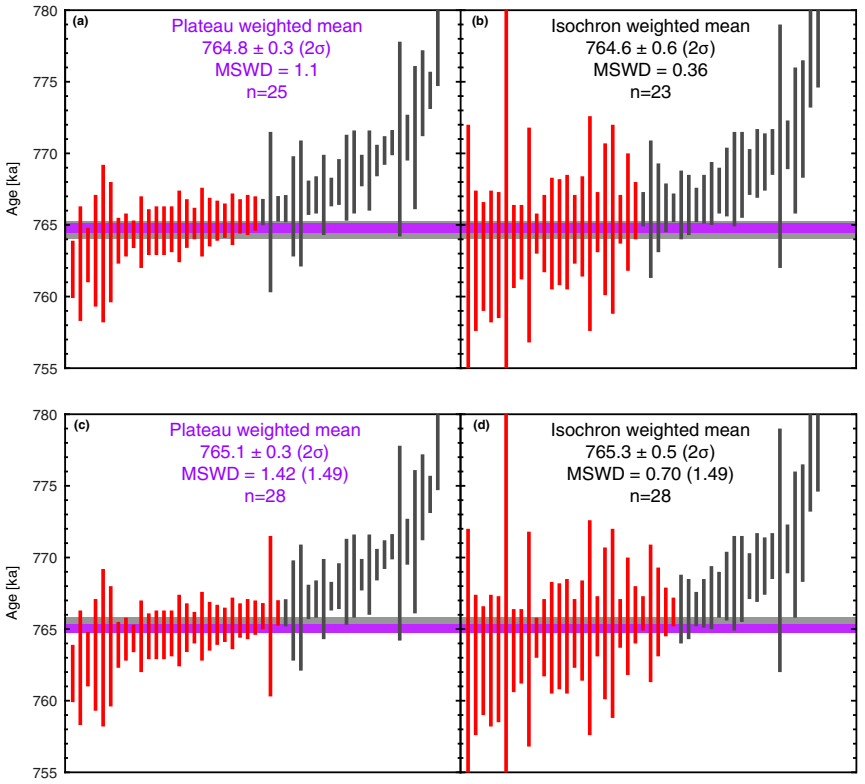

Fig. S3. Alternative calculation schemes for the BT eruption age. (*A* and *B*) Comparison of the weighted mean ages produced by the isochron and plateau dates. In each case, the youngest group of dates is defined as that for which the difference between the weighted mean and the next oldest date is greater than zero with 95% confidence. (*C*) Alternative weighted mean calculation which defines the youngest population as the largest group that yields an acceptable MSWD, less than 1.49 for $n = 28$. (*D*) The weighted mean of the isochron dates associated with the plateaus comprising the weighted mean in *C*.

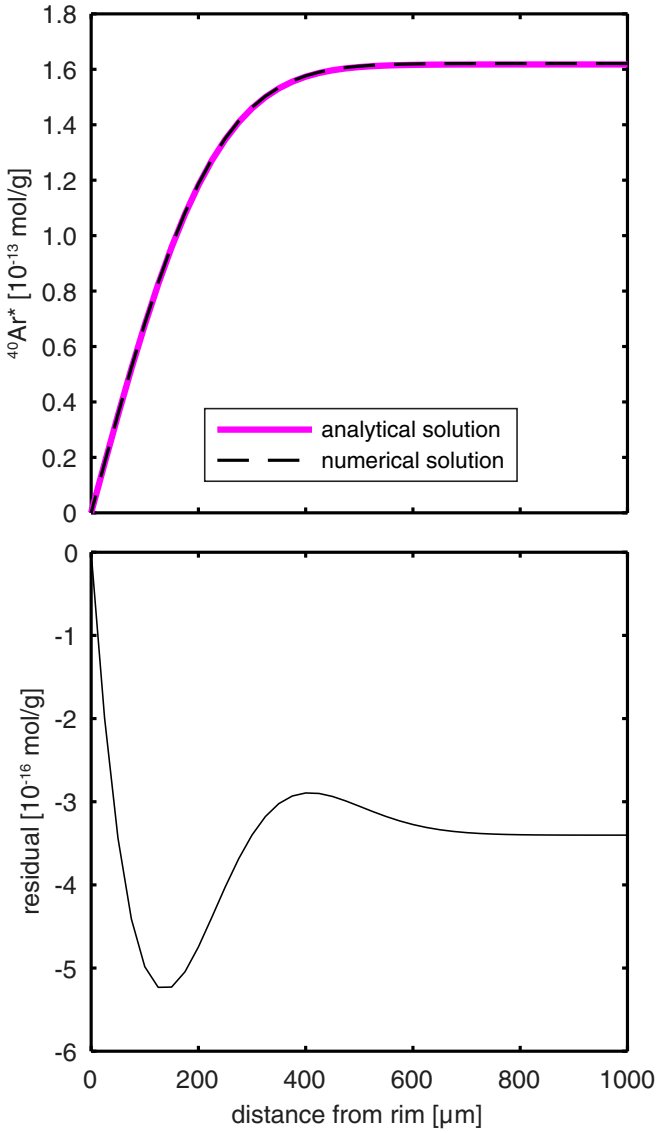

Fig. S4. Comparison of a 1D traverse of the numerical diffusion model result to an analytical solution. The initial condition for both calculations was 10 ky of ^{40}Ar* uniformly distributed in the crystal. The effects of diffusion were calculated for storage at 600 °C for 100 y. (*A*) Comparison of the numerical and analytical diffusion models. (*B*) The difference between the model results. Some of the small offset between the models is due to the analytical solution not accounting for the small amount of ^{40}Ar* ingrowth included in the numerical model.

Other Supporting Information Files

Dataset S1 (XLSX)
Dataset S2 (XLSX)
Dataset S3 (PDF)